# Impact of Competing Crystallization Processes on the Structure of All-Conjugated Donor–Acceptor Block Copolymers P3HT- b -PNDIT2 in Highly Oriented Thin Films

Viktoriia Untilova, Fritz Nübling, Laure Biniek, Michael Sommer, Martin Brinkmann

# Impact of competing crystallization processes on the structure of all-conjugated donor-acceptor block copolymers P3HT-*b*-PNDIT2 in highly oriented thin films

Viktoriia Untilova[1], Fritz Nübling[2], Laure Biniek[1], Michael Sommer[2] and Martin Brinkmann[1*]

(1) Institut Charles Sadron, CNRS-Université de Strasbourg, 23 rue du Loess, Strasbourg, 67034, France

(2) Makromolekulare Chemie und Freiburger Materialforschungszentrum, Universität Freiburg, Stefan-Maier-Straße 21, 79014 Freiburg, Germany.

(3) Institut für Chemie, Technische Universität Chemnitz, Straße der Nationen 62, 09111 Chemnitz, Germany

Corresponding authors: martin.brinkmann@ics-cnrs.unistra.fr

michael.sommer@chemie.tu-chemnitz.de

## Abstract

Mastering orientation and crystallization of all-crystalline, all-conjugated donor-acceptor diblock copolymers is of high interest for photovoltaic applications, as electronically beneficial nanostructuring of thermodynamically stable bulk heterojunctions can be achieved. Diblock copolymers composed of a regioregular poly(3-hexylthiophene) (P3HT) as donor and PNDIT2 as acceptor block were crystallized and oriented by epitaxy and high-temperature (HT) rubbing. The resulting highly oriented thin film structures were investigated in detail by transmission electron microscopy (electron diffraction and high resolution) and temperature-dependent polarized UV-vis absorption spectroscopy. Epitaxy and HT rubbing allow for selective crystallization and orientation of the blocks to obtain structures not accessible by standard spin coating and annealing processes. Epitaxy on trichlorobenzene allows for orientation and crystallization of P3HT, whereas additional annealing is necessary to crystallize the PNDIT2 block also. By contrast, HT rubbing aligns both blocks. The rubbing temperature controls the polymorphism (form I *versus* form II of PNDIT2), the orientation and the contact plane (edge-on *versus* face-on) of the backbones on the substrate. Crystallization of PNDIT2 constraints stacking of P3HT and modifies its unit cell parameters especially along the alkyl side chain direction. The lattice mismatch between the P3HT and PNDIT2 blocks hampers the growth of long-range highly ordered lamellar domains and results in highly disordered interfaces at the block junction. Overall, this study underlines the necessity to adapt layer spacings along alkyl side chains between donor and acceptor blocks to minimize unit cell mismatches and to enhance long range self-assembly into ordered lamellar donor-acceptor phases.

**Keywords**: block copolymers, organic photovoltaics, thin films, structure, transmission electron microscopy

## I. Introduction

Polymer semiconductors (PSCs) are key materials in the ongoing development of plastic electronics because their opto-electronic properties can be fine-tuned by chemical engineering, while their high solubility in organic solvents allows for low-cost and large-area processing.[1] Opto-electronic properties of PSC thin film devices can be further optimized by controlling polymer crystallization and orientation on substrates.[2] A face-on orientation of the conjugated backbone is ideal for efficient organic photovoltaics (OPV), whereas usually an edge-on orientation allows for two-dimensional in-plane charge transport in field effect transistors.[3-7] The most efficient organic solar cells make use of a donor copolymer fullerene acceptor blend, with power conversion efficiencies beyond 15 %.[8] While these mere numbers are exciting, the issue of unstable, kinetically trapped blend morphologies persists.[9,10] During operation of organic photovoltaic modules, further demixing towards thermodynamic equilibrium may occur which is detrimental to device performance.[11,12]

The power conversion efficiencies of all-polymer blends are catching up fast. These systems may have advantages related to slower phase separation compared to polymer fullerene blends.[12] However, the usual problem of polymer blend phase separation still exists for all-polymer solar cells. This is why recent efforts were dedicated to the synthesis of donor-acceptor block copolymers (BCP), which may self-assemble into well-defined nanostructured morphologies, given that several criteria related to the interaction parameter, molecular weight, block ratio and dispersity are met.[13-18] Moreover, especially attractive for OPV applications is that the block length defines the length scale of phase separation.[17] Thus, within the ordered region of the phase diagram, domain size can be adjusted by block length

according to the exciton diffusion length of the system, which is often on the order of ~10 nm.[19]

The phase diagrams of crystalline BCP with one or more crystalline blocks are more complex, as crystallization occurs in addition to phase separation. Numerous studies have been devoted to BCPs made of a conjugated block such as regioregular poly(3-hexylthiophene) (P3HT) and a non-conjugated chain bearing acceptor pendents such as perylene bisimide or fullerene.[15,20-23] In all-crystalline BCPs in general, covalent connectivity of the two blocks interferes with crystallization and brings about specific structural features observed in coil-coil and rod-coil systems. For instance, a rather strict structural constraint is imposed at the block junction of BCPs made of two crystallizable blocks with their own crystal lattices. Differences in unit cell parameters may impose chain tilts between the two blocks or disordered interfacial layers, as seen with polyolefine BCPs.[24] The sequential crystallization of two conjugated blocks has been investigated with conjugated BCPs made of poly(dioctylfluorene) and P3HT, but the relative packing of the two blocks and their mutual influence on crystallization was not assessed.[25,26] Even more appealing are BCPs based on P3HT and the n-type semiconductor poly{(N,N'-bis(2-octyldecyl)-1,4,5,8-naphthalene-dicarboximide-2,6-diyl]-alt-5,5'-(2,2'-bithiophene)}, referred to as PNDIT2. The morphology of P3HT-*b*-PNDIT2 in thin films was investigated using GIWAXS.[27-29] These studies demonstrated that both blocks can crystallize such that P3HT orients preferentially edge-on whereas PNDIT2 orients rather face-on on the substrate. Triblock copolymers P3HT-*b*-PNDIT2-*b*-P3HT were synthesized by Nakabayashi and Mori who showed that solar cells with power conversion efficiency of 1.28% can be obtained.[29] In all these cases, details of structure formation have not been addressed. More insight in the structure formation and block orientation on substrates was reported by *Yang et al.* for donor-donor BCPs of type poly(*p*-phenylene)-*b*-P3HT. The orientation of the PPP and P3HT on $SiO_2$, i.e. edge-on *versus*

face-on, can be controlled by choosing an appropriate crystallization temperature of the films. Yang *et al.* also proposed a mechanism of self-epitaxial crystallization of PPP on edge-on oriented P3HT to account for the mutual orientation of the two blocks on a substrate.[30]

Given the major importance of donor and acceptor chain and lattice orientation for photocurrent generation in blends of P3HT and PNDIT2,[31] BCPs not only offer unique opportunities in terms of thermodynamically stable morphologies, but additionally with respect to order, crystal orientation and interfacial design chain, all of which will strongly influence charge dynamics and photocurrent generation. Available studies on photovoltaically active, all-crystalline donor-acceptor BCPs including the above-mentioned details remain elusive but are key to a full understanding and further engineering of such materials with improved performance.

An elegant approach to address the structure of all-crystalline BCPs makes use of advanced orientation and crystallization methods such as epitaxy and high temperature (HT) rubbing. [32-37] Alignment of PSC is a powerful method to ease structural analysis of thin films as it helps to fix crystal orientation and polymorphism of the polymer. Epitaxy of PE-*b*-sPP helped understanding the relative orientation of the crystalline blocks depending on the crystallization conditions.[24] In this study, thin films of the all-conjugated, all-crystalline donor-acceptor P3HT-*b*-PNDIT2 are oriented and crystallized using epitaxy and HT rubbing. P3HT-*b*-PNDIT2 is made by direct arylation and carries an additional diketopyrrolopyrrole (DPP) unit at the block junction.[38-40] The DPP modulates interfacial charge dynamics but is not of importance for the structural investigations here. Using epitaxy and HT rubbing, we show that structures with different chain orientations can be obtained that are not accessible by conventional processing and annealing methods. Epitaxial crystallization of the BCP leads to face-on P3HT blocks and amorphous PNDIT2 blocks, whereas HT rubbing allows to orient both P3HT and PNDIT2 in a face-on manner. Depending on the rubbing temperature and

subsequent thermal annealing, edge-on orientations can also be achieved. Due to the mismatch in lattice parameters of P3HT and PNDIT2, P3HT segments at the interface are disordered and its lattice parameters significantly deviate from the ones of the P3HT homopolymer.

## II. Experimental section

**a)** The P3HT-*b*-PNDIT2 used here was synthesized by direct arylation polycondensation as reported elsewhere.[3] This BCP had a number average molecular weight of Mn,SEC= 42 kg/mol and a dispersity of 2.0 determined by SEC in chloroform (after Soxhlet extraction with methanol, acetone, ethyl-acetate and i-hexane). The weight fraction of P3HT was 42% (Estimated from $^1$H NMR integrals of side chain signals at 4.19 ppm (N-$CH_2$ of NDI) and 2.86 ppm (α-$CH_2$ of P3HT). The 1,3,5-trichlorobenzene (Aldrich) used for epitaxy was purified by sublimation.

### a) Oriented film preparation

Non-oriented films of P3HT-*b*-PNDIT2 were prepared by doctor blading from solutions in *ortho*-dichlorobenzene (*o*DCB) (5 wt % solution) on clean glass substrates. Mechanical rubbing of the copolymer films was performed following the methodology described in previous work.[31-33] In short, a microfiber cloth is applied at a pressure of 2-3 bar on the films. The rubbing length is 50 cm, the rotation speed of the cylinder is set at 300 rpm and the translation speed of the stage is 5 mm/s. The rubbing temperature is varied from ambient to 200°C and two rubbing cycles are used. The rubbing was performed under $N_2$ atmosphere (plaslab glove box) to avoid chemical degradation of the films. Post-rubbing annealing was performed in a Linkam LTS420 hot stage under $N_2$ atmosphere (20°C/min heating and cooling rates).

1,3,5-trichlorobenzene (TCB) was used as a crystallizable solvent for the directional solidification of the copolymers since TCB can orient both P3HT and PNDIT2 by epitaxy.[29,30] First, a thin film of the copolymer is prepared by drop casting (1wt% solution in chloroform) onto a clean glass slide. Upon addition of 10-25mg TCB powder and melting above 63°C, a uniform solution of the BCP/TCB is allowed to spread by capillarity between two glass surfaces. The whole is slowly moved on the Koeffler bench towards the colder part, until directional crystallization of TCB occurs. At this stage of the process, the colour of the sample turns from yellow-green to dark violet indicating that P3HT is crystallized subsequently to TCB. Finally, TCB is removed by slow evaporation at room temperature under primary vacuum leaving large areas (several $mm^2$) of oriented copolymer on the glass substrate.

**b) Thin film characterization.**

For Transmission Electron Microscopy (TEM) analysis, the copolymer films were coated with a thin amorphous carbon film evaporated using an Auto 306 evaporator (Edwards). Oriented areas were identified for TEM analysis by Polarized Optical Microscopy (POM) (Leica DMR-X microscope). The samples are then removed from the glass substrate by the polyacrylic acid method, floated on water and recovered on TEM copper grids. TEM was performed in bright field (BF), high resolution (HRTEM) and electron diffraction (ED) modes using a CM12 Philips microscope equipped with a MVIII (Soft Imaging System) Charge Coupled Device camera. Specific conditions for HR-TEM and low dose diffraction are given elsewhere.[32]

A Varian Carry 5000 UV- VIS-NIR spectrometer with polarized incident light was used to perform polarized UV-vis absorption spectroscopy. Temperature-dependent UV-vis spectroscopy was performed using a Linkam LTS420 hot stage with a temperature controller

T95-HS. For each temperature step, the sample's temperature was equilibrated for about 1 minute. The hot stage was purged continuously with $N_2$.

## III. Results and discussion.

### 1. Lamellar morphology and structure of P3HT-*b*-PNDIT2 induced by epitaxy and HT rubbing

The structure of P3HT-*b*-PNDIT2 (Figure 1.a) was investigated using oriented films prepared by epitaxy on trichlorobenzene (TCB) or by HT rubbing (Figures 1.b and 1.f, respectively). Both methods can orient the homopolymers P3HT and PNDIT2 very efficiently.[32,35] Figure 1.c-d and 1.g-h show polarized microscopy (POM) images of P3HT-*b*-PNDIT2 films oriented by epitaxy and by HT rubbing ($T_R$=175°C), respectively. The corresponding polarized UV-vis absorption of the films are shown in Figures 1.e and 1.i. Both films are birefringent in POM but their UV-vis absorption spectra are markedly different. In both cases, the UV-vis spectra is the sum of the P3HT and PNDIT2 contributions. The vibronic 0-0 and 0-1 components of P3HT are seen at 610 nm and 550 nm, respectively. Absorption at 710 nm and 400 nm stems from charge-transfer and $\pi$-$\pi^*$ absorption bands of PNDIT2, respectively. For the films oriented by epitaxy on TCB, only absorption of P3HT is clearly polarized, whereas the contribution from PNDIT2 does not exhibit anisotropy. In strong contrast, films oriented by rubbing at 175°C show strong polarization of both P3HT and PNDIT2. Films rubbed at 200°C show a dichroic ratio of 9.6 at 703 nm. Epitaxy on TCB orients only the P3HT block, whereas rubbing at 175°C-200°C can align both P3HT and PNDIT2.

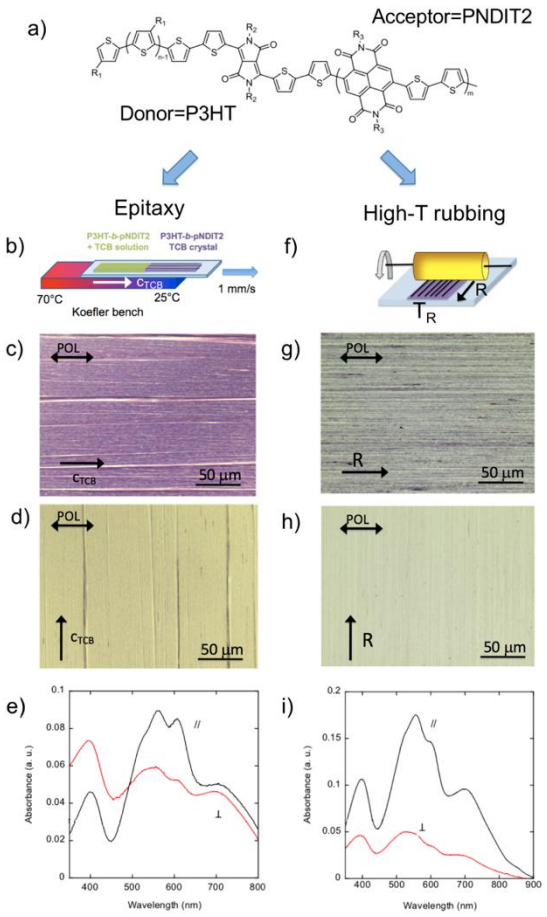


**Figure 1**. a) Chemical structure of the P3HT-*b*-PNDIT2 copolymer ($R_1$=$C_6H_{13}$, $R_2$=2-ethylhexyl, $R_3$=2-octyldodecyl) and schematic illustration of the orientation methods b) epitaxy and f) HT rubbing ($T_R$ is the rubbing temperature). c) and d) POM images of the films aligned by epitaxy on TCB for the light polarization parallel and perpendicular to the $c_{TCB}$ direction (noted by an arrow), respectively. e) polarized UV-vis spectra of epitaxied films on TCB. g) and h) POM images of the copolymer films oriented by HT rubbing at T=175°C for light polarization parallel and perpendicular to rubbing direction R. i) corresponding polarized UV-vis spectra for rubbed copolymer films. The arrow R indicates the rubbing direction.

Importantly, the comparison of the absorption spectra of rubbed films for POL//R and POL⊥R shows that P3HT is present in both crystalline and amorphous forms (Figures 1e,i).

Indeed, as shown for rubbed, semi-crystalline P3HT homopolymer films, the UV-Vis spectrum for POL⊥R is typical of amorphous interlamellar zones as it is strongly blue-shifted to 520 nm with only a slight contribution from the 0-0 vibronic component due to a small fraction of crystalline P3HT. This difference in polarized UV-vis absorption underlines differences in structure and orientation that were further visualized by TEM (Figure 2).

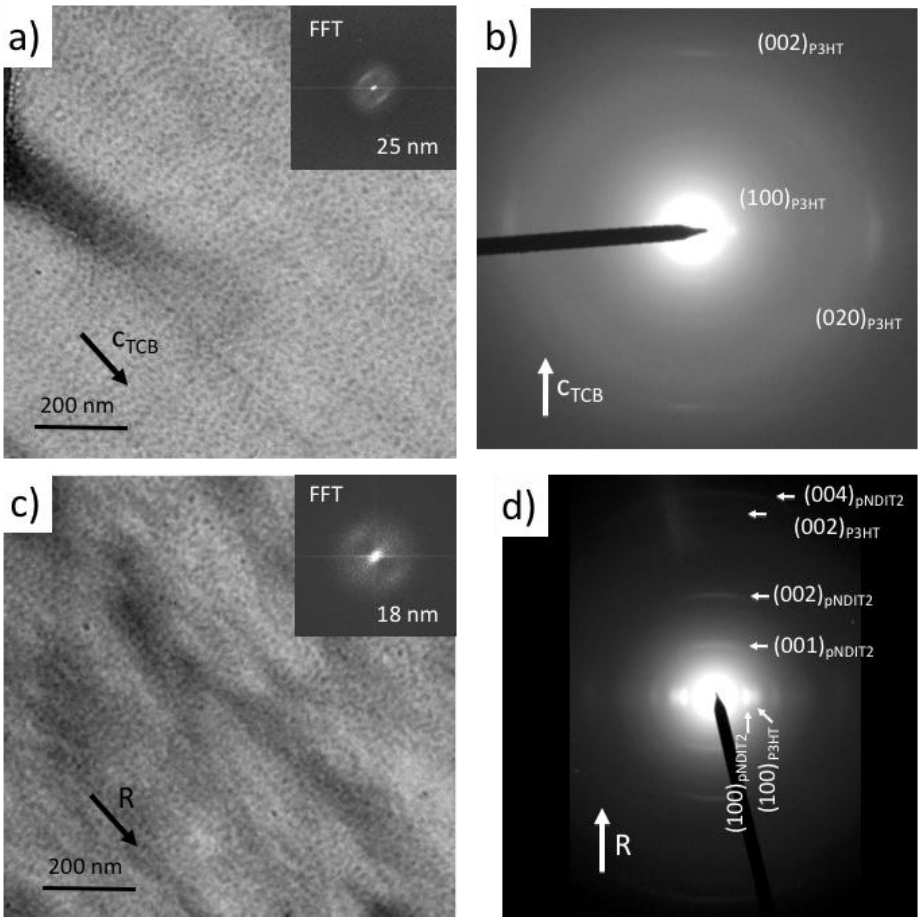


**Figure 2.** Bright field TEM images and electron diffraction pattern of oriented films of P3HT-*b*-PNDIT2 prepared by epitaxy (a, b) and HT rubbing at 175°C (c, d). The arrow in (a,b) corresponds to the c axis direction of the TCB substrate used for epitaxy. The arrow R in (c) and (d) correspond to the rubbing direction.

Figures 2a and 2c show representative bright field (BF) images of BCP films prepared by epitaxy and HT rubbing. In both cases, a long period $l_p$ is observed, but the value of $l_p$ depends on the preparation method: $l_p$ = 25±2 nm for epitaxied films and $l_p$= 18±1 nm for

films rubbed at 175°C. Importantly, both epitaxied and rubbed films of P3HT homopolymer of the same molecular weight also display a lamellar structure albeit with long periods different from the BCP (see Figure S1). For epitaxied films of the P3HT homopolymer, we observe $l_p$= 18±2 nm and for films rubbed at 175°C $l_p$= 15±2 nm. These values are consistent with a contour length $l_c$ = 16 nm (estimated from an absolute number average molecular weight $M_{n,NMR}$= 7 kg/mol) and suggest extended chain crystallization for the films prepared by epitaxy and therefore limited amorphous interlamellar zones.

In a first approximation that ignores the mutual impact of crystallization between the two blocks, the comparison of the lamellar periods of the BCP and P3HT homopolymer may give an indication of the extension of the PNDIT2 domains. In epitaxied films, the lamellar thickness of disordered PNDIT2 is ~ 7 nm (25 nm – 18 nm), whereas in films rubbed at 175°C, the extension of the PNDIT2 block should be ~ 3 nm. As seen hereafter using High Resolution Transmission Electron Microscopy (HRTEM) and electron diffraction (ED), the extension of ordered P3HT and PNDIT2 domains in the BCP is different from this simplistic image because the constrained crystallization between both blocks due to lattice mismatches induces disordered interfaces at the block junction (vide infra).

Further differences in the structure of oriented BCP films prepared by the two methods are evidenced by electron diffraction (ED). Figures 2b and 2d show the ED patterns of epitaxied and HT rubbed BCP films, respectively. Table 1 collects the reticular distances of the characteristic reflections. In epitaxied films, the coexistence of equatorial $100_{P3HT}$ and $020_{P3HT}$ reflections indicates a mixture of face-on and edge-on crystals of P3HT. Although the pattern shows a well-defined $002_{P3HT}$ meridional reflection, mixed reflections are absent in contrast to epitaxied films of P3HT homopolymer (see Figure S1). This implies that crystalline order of epitaxially grown BCP films is lower than for the P3HT homopolymer. This is further confirmed by differential scanning calorimetry (DSC) indicating a markedly

lower degree of crystallinity for BCPs versus homopolymer (see Supporting information Figure S2). The melting enthalpy of the P3HT block in the BCP is only 70 % of the P3HT homopolymer. In accordance with polarized UV-vis spectroscopy, the ED pattern of epitaxied P3HT-*b*-PNDIT2 does not show reflections corresponding to PNDIT2, suggesting that the PNDIT2 block is amorphous. Again, this is in agreement with the absence of orientation deduced from polarized UV-vis spectroscopy. Accordingly, epitaxy of P3HT-*b*-PNDIT2 on TCB results in the selective crystallization and orientation of the P3HT block only (Figure 3.a).

In strong contrast, the ED pattern of oriented films prepared by rubbing at 175°C shows contributions of both P3HT and PNDIT2 blocks. The $100_{PNDIT2}$ and $100_{P3HT}$ reflections observed on the equator indicate that both blocks have a dominant face-on orientation with their backbone aligned along the rubbing direction (see Figure 3.b). Along the meridian, the ED pattern is dominated by the intense $00l_{PNDIT2}$ with $l$ = 1, 2 and 4 of the PNDIT2 block, whereas only a weak $002_{P3HT}$ is seen for P3HT. The relative intensity of the $00l_{PNDIT2}$ reflections indicate that this block crystallizes in form I, i.e. with segregated stacks of NDI and T2.[34,35] As a whole, this ED pattern is characteristic of an oriented block copolymer film with both P3HT and PNDIT2 blocks oriented mainly face-on the substrate (see Figure 3.b). Accordingly, epitaxy and HT rubbing allow to control the crystallization of the two blocks in different manners.

To further reveal the influence of the PNDIT2 block on the crystallization of the P3HT block, the ED pattern of the oriented BCP was compared with that of the P3HT homopolymer. In epitaxied films of the P3HT homopolymer, $d100_{P3HT}$ = 15.7 Å *versus* 16.9 Å-17.0 Å for the BCP (see Figure S1). Moreover, multiple orders of sharp $h00_{P3HT}$ ($h$=1, 2, 3) reflections are seen for the P3HT homopolymer while only one blurred and fuzzy $100_{P3HT}$ reflection is visible for the BCP. Accordingly, our ED data indicate that the P3HT lattice is

substantially expanded along the alkyl side chains in the BCP with a broad distribution of $d100_{P3HT}$ layer spacings as compared to the homopolymer. Both observations suggest that the P3HT block crystallization is modified by the presence of the crystalline PNDIT2 block. This can be understood in terms of lattice mismatch at the block junction between the PNDIT2 and the P3HT blocks. As illustrated in Figure 3.b, the distance between layers of π-stacked chains is 23.3 Å for the PNDIT2 block ($T_R$=150-175°C) *versus* 17-18 Å for the P3HT block. The lattice expansion along the alkyl side chains is therefore the response of the P3HT block to the presence of the crystalline PNDIT2 block.

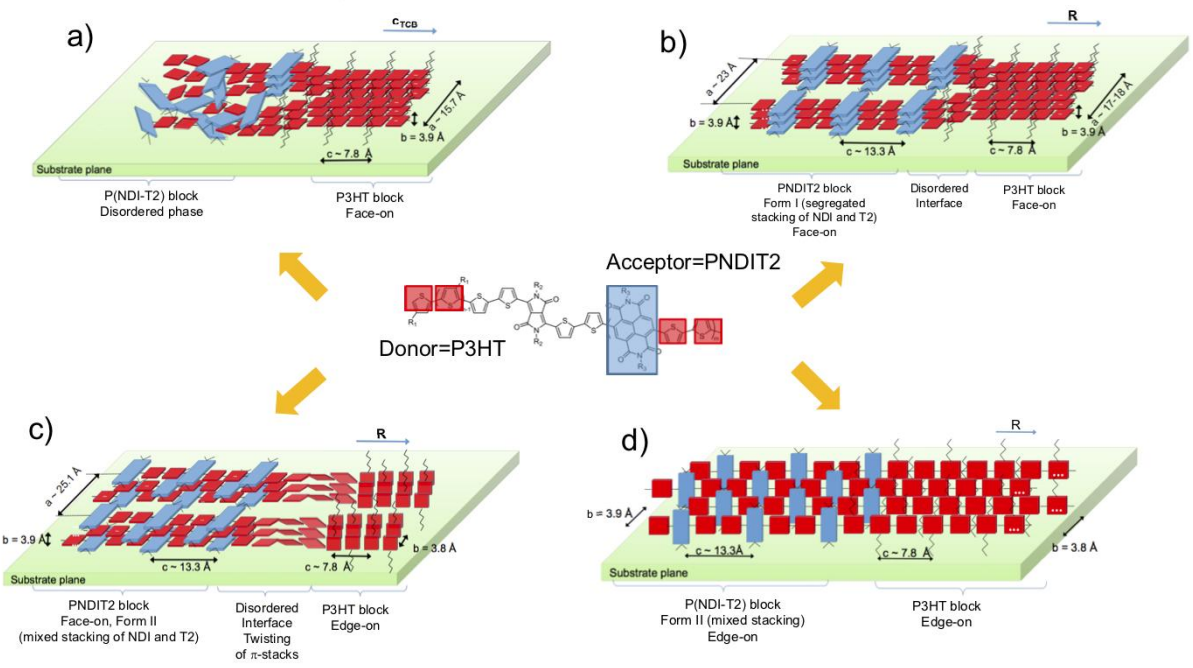


***Figure 3****. Summary of representative orientations and structures of aligned P3HT-b-PNDIT2 thin films prepared under different orientation and crystallization conditions. (a) BCP films with face-on P3HT and disordered PNDIT2 blocks are observed for epitaxy on 1,3,5-trichlorobenzene,(b) BCP films with both face-on P3HT and face-on PNDIT2 blocks are found in the case of rubbed thin films for 150°C≤$T_R$≤175°C,(c) BCP films with face-on PNDIT2 and edge-on P3HT blocks and a disordered interface are observed in rubbed films*

*for $T_R \geq 200°C$ (d) BCPs films with both edge-on P3HT and PNDIT2 blocks are preferentially formed for high annealing temperatures after melt-crystallization of P3HT ($T_A$=250°C) .*

Although ED is powerful to highlight structural features such as polymorphism and contact planes, it cannot visualize the way the blocks organize one with respect to the other or the type of interface between the two blocks. Therefore, low dose high resolution TEM (HRTEM) was used to probe the film nanomorphology in real space. Figure 4 shows a representative HRTEM image of a block copolymer film oriented by HT rubbing ($T_R$=200°C) as well as an enlarged view of the disordered interface between a PNDIT2 and a P3HT block in face-on orientation. The HRTEM images show fringed patterns that are typical of face-on crystals. The remaining of the film surface without fringed patterns corresponds to either disordered domains or edge-on blocks with a stacking period not observable by HRTEM. The fast Fourier transform (FFT) of the HRTEM image consists of two sets of broad and fuzzy reflections corresponding to $100_{PNDIT2}$ and $100_{P3HT}$ ($d100_{PNDIT2}$=23.3 Å and $d100_{P3HT}$=16.8 Å for P3HT). Both reflections in the FFT are very broad and similar to those seen in the ED patterns. This is in strong contrast to the FFTs of HRTEM images of the homopolymers that show a much better defined $100_{P3HT}$ layer period.[32]

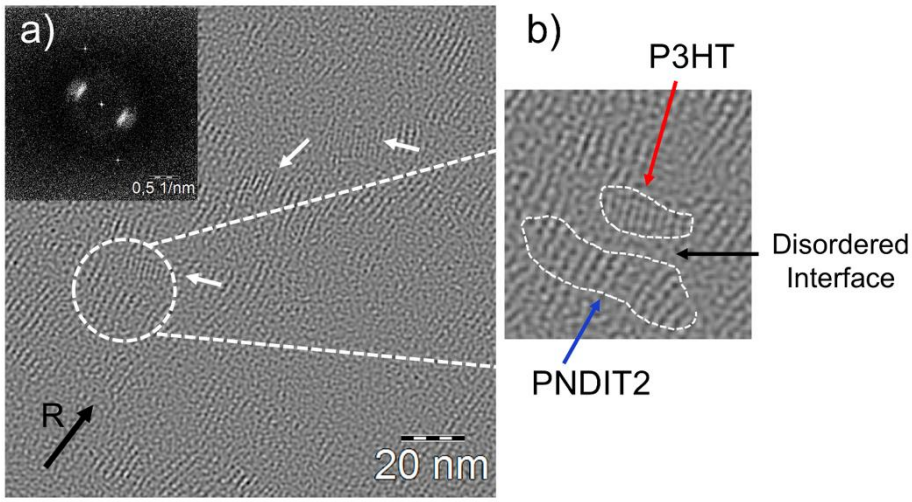

***Figure 4****. a) Representative low dose high resolution TEM image of an oriented block copolymer film obtained by rubbing at 200°C showing mainly face-on crystalline PNDIT2 domains. The inset corresponds to the FFT. Note the coexistence of two fuzzy reflections corresponding to broadened* $100_{PNDIT2}$ *and* $100_{P3HT}$ *in the FFT. The white arrows highlight P3HT crystals with a lattice period of 16.8 Å. b) enlarged image showing two crystalline stacks of P3HT and PNDIT2, respectively, and disordered regions in between them.*

In the HRTEM image of rubbed films at 200°C (Figure 4), a majority of face-on PNDIT2 domains is observed and only a small fraction of the surface corresponds to face-on P3HT domains (highlighted by white arrows in Figure 4.a). The crystal size is larger for PNDIT2 than for P3HT. The average stem length in both blocks can be roughly estimated from a statistic on HRTEM images: ~ 5-6 nm (13-15 monomers) in P3HT *versus* 7-8 nm (5-6 monomers) in PNDIT2. Importantly, HRTEM additionally indicates that the crystalline P3HT and PNDIT2 domains are not adjacent but rather separated by disordered interfacial areas several nanometers wide. This agrees well with the signature of amorphous P3HT fraction in the UV-vis absorption spectra of the rubbed films (POL⊥R) and the lower degrees of crystallinity determined by DSC (see Figure S2). It is also interesting to note that the dimension of the P3HT crystals along the side chains i.e. along $\mathbf{a_{P3HT}}$ is more limited in the copolymer than in the P3HT homopolymer.[36] Oriented P3HT homopolymers of low $M_n$= 7.0 kg/mol show face-on crystals with large dimensions along the side chain direction.[36] This limited growth of the P3HT domains along $\mathbf{a_{P3HT}}$ is due to the constraints on crystallization imposed by the PNDIT2 block.

**Table 1.** Reticular distances in rubbed thin films of P3HT-*b*-PNDIT2 as a function of rubbing temperature $T_R$ and for a rubbed film after annealing at 250°C.

| Sample | $d100_{PNDIT2}$ (Å) | $d100_{P3HT}$ (Å) | $d002_{P3HT}$ (Å) | $d_{\pi}$ (Å) | $d001_{PNDIT2}$ (Å) | $d002_{PNDIT2}$ (Å) |
|---|---|---|---|---|---|---|
| Epitaxy TCB | - | 15.6-16.0 | 3.85 | - | - | - |
| Annealed 100°C | - | 15.50 | 3.85 | - | 13.6 | - |
| Annealed 200°C | 25.5 | 17.7 | 3.85 | 3.8 | 13.7 | 6.9 |
| Annealed 250°C | 25.1 | - | - | 3.8 | - | 6.9 |
| Rubbed films | | | | | | |
| 150°C | 22.2 | 17.7 | 3.85 | - | 13.6 | 6.9 |
| 175°C | 23.7 | 16.8 | - | - | 13.7 | 6.9 |
| 200°C | 23.5 | 16.8 | - | - | 13.5 | 6.9 |
| Annealing 250°C | 25.1 | 16.9 | - | 3.9/3.8 | 13.5 | 6.95 |

**2. Control of polymorphism and orientation in rubbed and epitaxied films**

Hereafter, we show that the crystal structure and orientation in both epitaxied and rubbed films of the BCP can be further manipulated by thermal annealing and/or by adjusting the rubbing temperature.

### a) Rubbed thin films of P3HT-*b*-PNDIT2: impact of rubbing temperature $T_R$.

Two means are used to control the polymorphism and contact plane of the blocks on the substrate, namely by adjusting the rubbing temperature or by additional thermal annealing.

First, the effect of rubbing temperature $T_R$ is considered. Similarly, for the homopolymers P3HT and PNDIT2, the dichroic ratio (DR) of the absorption bands characteristic of both blocks increases with increasing $T_R$ (See Figure S3). Typically, at the peak maximum of the PNDIT2 block, DR increases from 2.8 at 125°C to 9.6 at 200°C, indicating that alignment improves with $T_R$. The same is observed for the characteristic absorption band of the P3HT block, but at 200°C the DR remains lower (DR= 5) (see Figure S3).

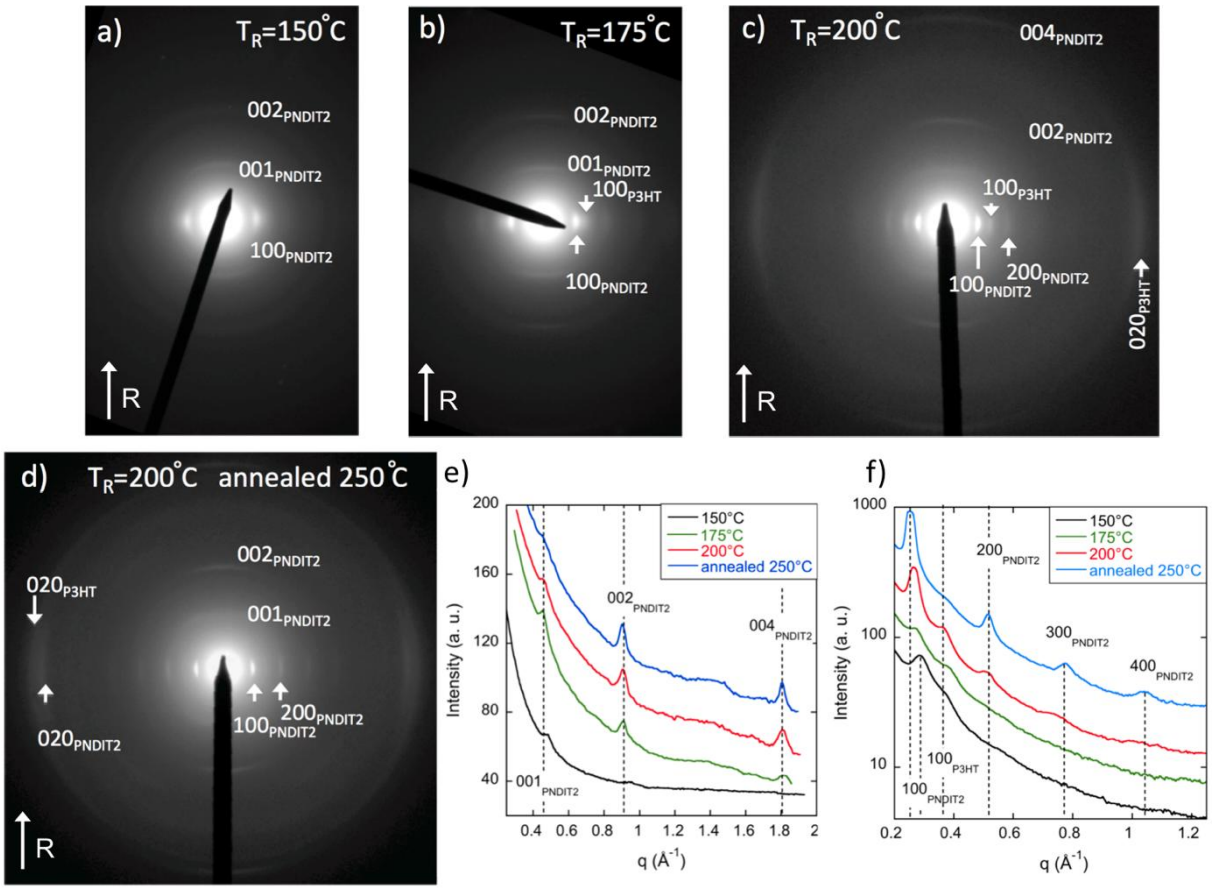


**Figure 5**. Evolution of the electron diffraction pattern of rubbed P3HT-*b*-PNDIT2 copolymer films as a function of the rubbing temperature $T_R$. (a) $T_R$=150°C, (b) $T_R$=175°C, (c)

$T_R$=200°C and (d) ED pattern of a copolymer film rubbed at 200°C after annealing at 250°C (1 min.). For all ED patterns, the rubbing direction is vertical and noted by a white arrow (R). (e) and (f) Plot profiles of the ED patterns along the meridian and the equator, respectively. Note the shifts of the $100_{PNDIT2}$ and the $100_{P3HT}$ peak positions with $T_R$.

The TEM analysis indicates that $T_R$ not only improves in-plane orientation but modifies substantially the structure of the films. The evolution of the electron diffraction patterns of rubbed films versus $T_R$ is shown in Figure 5 as well as the section profiles along the equator and the meridian of the ED patterns. For $T_R$=150°C, the ED pattern is dominated by reflections characteristic of face-on aligned PNDIT2 blocks. The stronger intensity of the meridional $001_{PNDIT2}$ over $002_{PNDIT2}$ indicates that the PNDIT2 block crystallizes in form I i.e. with segregated stacks of NDI and bithiophene (see Figure 3.b).[34,35] The P3HT block shows only a very fuzzy equatorial $100_{P3HT}$ reflection with $d100_{P3HT}$=17.7Å (see Figure 5.a and 5.f). This value is significantly larger than the expected 15.7 Å for a 7 kDa P3HT homopolymer. Both observations underline the constrained crystallization of P3HT which remains highly disordered for $T_R$=150°C.

Increasing $T_R$ results in the following important changes: (i) the $100_{PNDIT2}$ peak becomes sharper, (ii) $d100_{PNDIT2}$ shifts to larger values (23.5 Å for $T_R$=200°C *versus* 22.2 Å for $T_R$=150°C), (iii) $d100_{P3HT}$ shifts to smaller values and gets slightly better defined and (iv) the meridional $002_{PNDIT2}$ becomes more intense than the $001_{PNDIT2}$. As a result, the ED pattern for $T_R$=175°C is characteristic of the coexistence of face-on crystals of form II PNDIT2 and face-on crystals of P3HT (the intensity of $002_{PNDIT2}$ exceeds clearly that of $001_{PNDIT2}$ and this is the fingerprint of form II PNDIT2).[34,35] When $T_R$ reaches 200°C , the equatorial *h*00 (*h*=1,2) tend to disappear at the expense of the equatorial $020_{P3HT}$ reflection, suggesting that the fraction of edge-on P3HT becomes more important. At the same time, the PNDIT2 block

stays face-on. This is also consistent with the trend observed for P3HT homopolymers for which low $T_R$ (< 150°C) results in pure face-on domains whereas mixtures of face-on and edge-on crystals are seen at higher $T_R$. [32,37] If the BCP domains are made of face-on PNDIT2 and edge-on P3HT, it implies that the backbones of both blocks are orthogonal to another. This situation leads to a strong lattice incompatibility at the interface between the two blocks and results necessarily in disordered interfaces at the block junction. How is it possible to change from the 25.1 Å interchain in-plane periodicity of the face-on PNDIT2 block to the 3.8 Å in-plane periodicity of the edge-on P3HT block? As seen in Figure 3.c, we propose that a collective twisting of the P3HT chains within a π-stacks close accounts for the face-on to edge-on transition between blocks. A set of 6-7 π-stacked P3HT chains originally in face-on orientation has a total thickness of 6-7 x 3.8 Å = 22.8 -26.6 Å along the π-stacking direction that is close to the 25.1 Å distance between two π-stacks of the face-on PNDIT2. Hence, by twisting the P3HT chain orientation along the chain axis, it is possible to transform a face-on π-stack of P3HT to an edge-on stack of P3HT while respecting the original distance between PNDIT2 π-stacks of 25.1 Å.

Further control of structure in the rubbed BCP films can be achieved by thermal annealing after orientation. The ED pattern of a rubbed BCP film ($T_R$=200°C) after annealing at 250°C is shown in Figure 5.d. It features the characteristic reflections of form II of PNDIT2 with a dominant face-on orientation of the crystals that are still perfectly aligned in-plane. However, on the equator of the ED pattern, two characteristic π-stacking reflections at 3.8 and 3.9 Å must be attributed to oriented edge-on domains of P3HT and PNDIT2, respectively. This indicates that annealing has fully reoriented the P3HT block from face-on in the rubbed films ($T_R$=200°C) to edge-on whereas both face-on and edge-on PNDIT2 blocks are observed (although face-on PNDIT2 is dominant). Accordingly, in such films, it is possible to find

BCP domains as shown in Figure 3.c with orthogonal block orientations and also fully edge-on BCP domains as shown in Figure 3.d.

From a morphological point of view, the BF image in Figure S4 indicates that the oriented lamellar morphology is only seen for $T_R \geq 175°C$, whereas for 150°C a disordered phase-separated-like morphology is observed. The rubbing temperature impacts the total lamellar periodicity which tends to increase with $T_R$ from 18.3±0.5 nm at 175°C to 22.2±0.5 nm for 200°C. This increase in total lamellar periodicity is consistent with the increase of lamellar period in P3HT homopolymers with $T_R$. [28] For films annealed at $T_A$=250°C, the films also show a periodic lamellar morphology but with a strong increase of periodicity to 33 nm. This value is about twice the contour length of the BCP chains and could suggest formation of a non-interdigitated double layer lamellar packing. Such a situation has been reported earlier for poly(styrene)-poly(ethylene oxide) copolymers.[41,42]

**a) Tuning the block contact plane and polymorphism in epitaxied thin films**

Having demonstrated that epitaxy of P3HT-*b*-PNDIT2 promotes alignment of the only P3HT block while the PNDIT2 block remains in a disordered phase, it was natural to attempt to manipulate further the structure of the BCP films by thermal annealing. Figure 6 shows a sequence of ED patterns of the oriented films as a function of $T_A$ and the section profile along the meridian of the ED patterns (Figure 6.d).

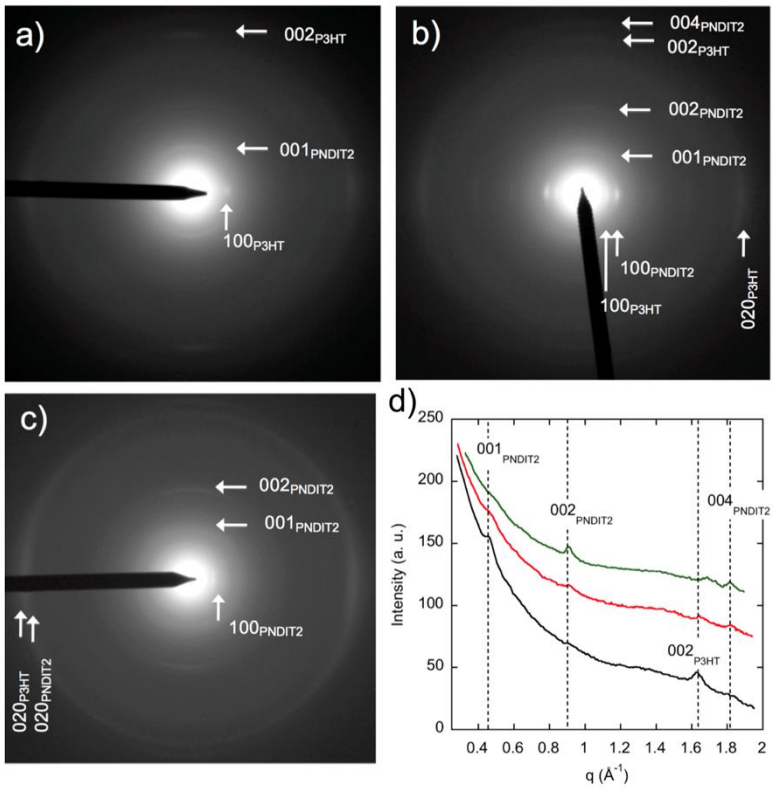


**Figure 6**. Evolution of the diffraction pattern in P3HT-*b*-PNDIT2 copolymer films oriented by epitaxy as a function of the annealing temperature $T_A$ (1 min). a) $T_A$=100°C, b) $T_A$=200°C and c) $T_A$=250°C. d) Meridional section profiles of the ED patterns for $T_A$=100°C (black), $T_A$=200°C (red) and $T_A$=250°C (green).

The impact of thermal annealing bears some similarity with that observed for increasing rubbing temperature $T_R$. Only crystallized P3HT blocks are present in as-epitaxied films. After annealing at 100°C, the $001_{PNDIT2}$ reflection appears on the meridian, indicating that the segregated stacking of NDI and T2 units of the PNDIT2 block sets in (form I). Importantly, there is no evidence for a layered structure of PNDIT2 since the $100_{PNDIT2}$ is not visible on the equator. This observation is important as it shows that the crystallization of PNDIT2 starts with segregation of NDI and T2 units that π-stack, whereas the growth of the layered structure with alternation of π-stacked backbones and alkyl side chains is observed only at higher $T_A$ around 200°C. As seen in Figure 6, the $100_{PNDIT2}$ reflection appears on the

equator only for $T_A$=200°C. This indicates that the π-stacked chains of PNDIT2 further organize to form a layered structure with a periodicity $100_{PNDIT2}$=23.5 Å. In parallel, the strong intensity of the meridional $002_{PNDIT2}$ indicates that the mixed stacking of T2 and NDI (form II) is obtained for $T_A$=200°C. Although the meridional $002_{P3HT}$ reflection is still present, it is reduced in intensity and arced, indicating a loss of order along the backbone and also a loss of in-plane orientation. A drastic change in the ED pattern is observed at 250°C when $T_A$ is beyond the melting temperature of the P3HT block. As seen in Figure 6, the ED pattern does not show any of the initial reflections characterizing epitaxied P3HT. The only reminiscence of crystalline P3HT is a Scherrer-like ring at $020_{P3HT}$=3.8 Å with equatorial intensity reinforcement that indicates the reorientation of the P3HT blocks to edge-on and partial loss of in-plane orientation. Besides, ED shows the characteristic reflections of face-on PNDIT2 in form II. Accordingly, when the epitaxied P3HT films are annealed above the melting of P3HT, a full reorganization of the P3HT block to edge-on is observed along with crystallization of the PNDIT2 block in form II with dominant face-on orientation. The two blocks of the copolymer show orthogonal π-stacking directions which must imply a large disordered interfacial layer between the two blocks (Figure 3c). This situation is similar to that observed for blends of P3HT and PNDIT2 after melt crystallization of the P3HT block, but in the present case, the two blocks are linked together, which results in a strong frustration in block orientation.[32]

To summarize, the different orientations and polymorphs of P3HT-*b*-PNDIT2 films that are obtained by epitaxy and HT rubbing are collected in Table 2. Further insight in the sequential crystallization of the P3HT and PNDIT2 blocks is obtained from a study of the thermochromism using T-dependent UV-vis absorption spectroscopy.

**Table 2**. Summary of main block orientations with respect to the substrate (contact plane) as a function of the film preparation method and annealing conditions.

| **Epitaxy** | | **Rubbing** | |
|---|---|---|---|
| as-cast films | Face-on+Edge-on P3HT<br>Disordered PNDIT2 | - | - |
| $T_A$=100°C | Face-on+Edge-on P3HT<br>Face-on PNDIT2 (form I) | $T_R$=150°C | Disordered P3HT block<br>Face- on PNDIT2 (form I) |
| $T_A$=200°C | Edge-on P3HT<br>Mainly Face-on PNDIT2 (form II) | $T_R$=175°C | Face-on P3HT<br>Face-on PNDIT2 (form I) |
| $T_A$=250°C | Edge-on P3HT<br>Mainly Edge-on PNDIT2 (form II) | $T_R$=200°C | Edge-on P3HT<br>Face-on PNDIT2 (form II) |
| - | - | $T_R$=200°C<br>+ annealing ($T_A$=250°C) | Edge-on P3HT<br>Edge-on + Face-on PNDIT2 (form II) |

### 3. Thermochromism of P3HT-*b*-PNDIT2

Orientation and alignment of the two blocks is corroborated by temperature-dependent optical properties of P3HT-*b*-PNDIT2. Most conjugated polymers show a marked thermochromism that is related to the conformational changes from planarized chain segments in the crystalline phase to non-planar, coiled-like conformation in the melt phase.[43,44] In P3HT, thermochromism is manifested by the color change from violet to orange when temperature is increased from ambient temperature to 240-250°C. The fact that the P3HT and the PNDIT2 blocks show distinct absorption bands and different melting temperatures allows the observation of these processes separately. Figure 7 shows the evolution of UV-vis absorption spectra of a rubbed thin film of the P3HT-*b*-PNDIT2 copolymer ($T_R$=200°C) as a

function of the annealing temperature for both heating and cooling cycles (Figure 7a and 7b, respectively). To preserve in-plane alignment, heating was limited to the melting temperature of P3HT i.e. 250°C.

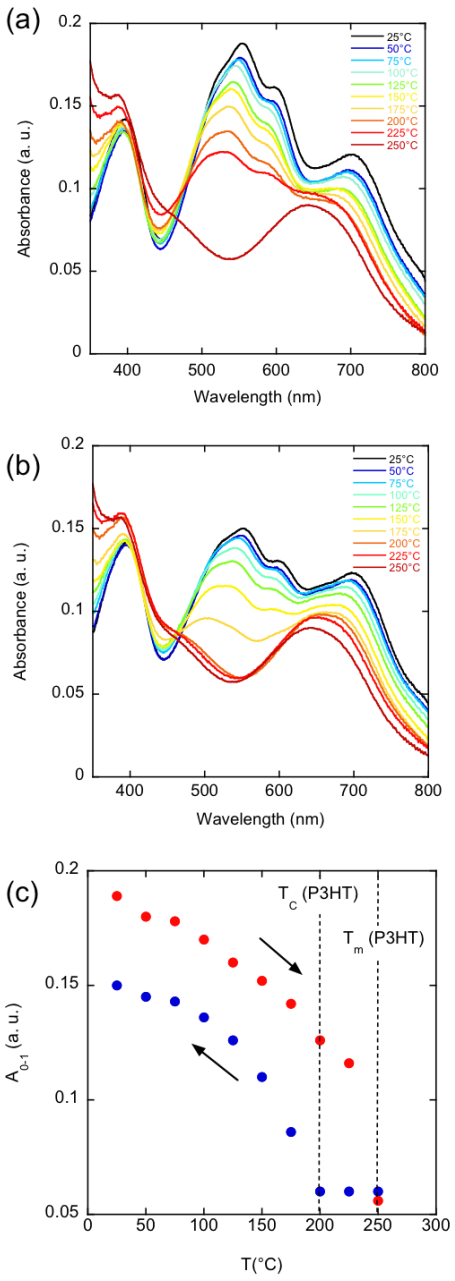


**Figure 7**. Evolution of UV-vis absorption spectra of rubbed P3HT-*b*-PNDIT2 ($T_R$=200°C) as a function of temperature : (a) heating cycle and (b) cooling cycle. (c) Plot of the absorbance of the 0-1 vibronic band of P3HT block as a function of temperature upon heating (red dots) and cooling (blue dots).

First, heating results in a blue-shift of both the absorption bands of the P3HT and the pNDIT2 blocks. For P3HT, the 0-1 component of the vibronic structure shifts from 554 nm at 25°C to 529 nm at 225°C. The melting of the P3HT block between 225°C and 250°C results in a collapse of the absorption band of the P3HT block and a corresponding change in the film colour from violet to green. In parallel, heating results in the blue shift of the PNDIT2 absorption from 702.5 nm at RT to 678 nm at 225°C. This blue shift is explained by the decrease in backbone planarity of PNDIT2 with increasing temperature.

Upon cooling, the thermochromism is partly reversible in the sense that the initial absorbance of the P3HT is only partially recovered. After cooling to 25°C, the UV-vis absorption of the PNDIT2 block is red-shifted back to 699 nm, i.e. close to the original position. The final absorbance is almost identical to the initial value. This implies that the in-plane orientation of the PNDIT2 block is maintained after thermal annealing of the films at 250°C. For P3HT, the situation is different. For POL//R, the final absorbance is lower after annealing than the absorbance prior to annealing. The opposite is observed for POL⊥R (see supporting information, Figure S5). This indicates that alignment of the P3HT block is partially lost after annealing. Comparing the temperature dependence of the 0-1 vibronic band upon heating and cooling evidences a hysteresis as seen in Figure 7c. This hysteresis is consistent with the DSC data for the copolymer (see SI Figure S2) and reflects the difference between the melting and crystallization temperatures of the P3HT block at 224°C and 169°C, respectively.

The changes in absorbance of the copolymer films after annealing to 250°C suggest reorientation of the P3HT block in accordance with electron diffraction. In Figure 6.c, the ED pattern shows that the equatorial $(100)_{P3HT}$ reflection has almost fully disappeared whereas a strong and broad $(020)_{P3HT}$ developed on the equator. This indicates a reorientation

mechanism of P3HT block from initially face-on in as-rubbed films to fully edge-on after melt-crystallization of the P3HT block. The $(020)_{P3HT}$ peak also shows a large in-plane angular spread after annealing at 250°C, which is consistent with the loss of in-plane chain orientation evidenced by polarized UV-vis absorption. Beside the reflections of P3HT, the intense $(100)_{PNDIT2}$ and $(002)_{PNDIT2}$ indicate that substantial face-on domains of form II PNDIT2 is present in the films after thermal annealing to 250°C. However, a population of edge-on crystals of PNDIT2 is also present as indicated by the presence of the equatorial $(020)_{PNDIT2}$.

**III. Discussion**

Alignment and controlled sequential crystallization of the all-conjugated, all-crystalline donor-acceptor block copolymer P3HT-*b*-PNDIT2 was achieved by epitaxy and HT rubbing. Epitaxy on crystalline TCB leads to selective crystallization and orientation of the P3HT block. HT rubbing at $T_R \geq 175$°C or thermal annealing at $T \geq 200$°C promotes the crystallization of the PNDIT2 block (form II) along with a constrained crystallization of the P3HT block. The fact that only the P3HT segment of P3HT-*b*-PNDIT2 is oriented by epitaxy on TCB is *a priori* surprising since both blocks taken individually can be oriented that way.[33,34] For the P3HT block, it has been demonstrated that 1D epitaxy explains alignment since $c_{TCB} \approx c_{P3HT}/2$.[33] The absence of epitaxial crystallization and orientation of PNDIT2 on TCB can be explained by considering two possibilities. Firstly, if epitaxy of the P3HT block sets in first, it then imposes registry in direction and position of the copolymer chains on the TCB substrate. However, once the position of the P3HT block is fixed by 1D epitaxy on TCB, the PNDIT2 segment is unable to find an optimal position and remains disordered. Such situation was observed with PE-*b*-sPP, for which the crystallization temperature dictates the sequence of crystallization of the two blocks. The first block that crystallizes imposes the

orientation of the copolymer on the substrate.[24] A second possibility is simply that TCB is a preferential solvent of the PNDIT2 block. In that case, when P3HT crystallizes by epitaxy, the remaining PNDIT2 domains are still swollen by TCB and finally solidify without crystallizing. This would explain the absence of crystallization and orientation of the PNDIT2 block on TCB.

The situation regarding rubbed films of P3HT-*b*-PNDIT2 is different, since rubbing tends to align both blocks parallel to the rubbing direction. The rubbing temperature determines the dominant contact plane of the blocks. For $150°C \leq T_R \leq 175°C$, both blocks align parallel to the rubbing and the crystalline domains tend to orient mainly face-on the substrate. However, ED shows that the crystallization of the PNDIT2 block significantly constrains the lattice of P3HT whose unit cell expands along $\mathbf{a_{P3HT}}$ (alkyl side chains). Moreover, the $(100)_{P3HT}$ reflection is very broad and fuzzy suggesting a large distribution of inter-layer spacings $\mathbf{a_{P3HT}}$. Obviously, the layer spacings along the alkyl side chains are significantly different for PNDIT2 and P3HT: $a_{PNDIT2}$=23.5-25.0 Å and $a_{P3HT}$=16.0-16.8 Å. Accordingly, this is clear evidence for the incompatibility in the crystallization of both blocks that is a consequence of the lattice mismatch between the two blocks at the block junction (see Figure 4). This leads to disordered interfacial zones, which can be directly visualized by HRTEM. Figure 4.a shows that oriented, crystalline P3HT stems are not located directly at the interface with PNDIT2 stems but separated by a disordered interfacial interlayer. This is consistent with UV-vis spectroscopy data for POL⊥R that evidence the presence of amorphous P3HT as well as DSC which confirms a lower degree of crystallinity compared to homopolymers.

A second origin of highly disordered interfacial layers between the P3HT and PNDIT2 blocks can be found when one block is in face-on and the second in edge-on orientation on the substrate (films rubbed at 200°C and annealed at 250°C). As seen previously, a possible twisting of the π-stacks may occur between the two blocks to change the contact plane. It may

be anticipated that such disordered interfacial layers lower the efficiency of charge separation at the block junction, and hence are detrimental for the efficiency of photovoltaic devices. This is further consistent with the reported decrease in device efficiency in solar cells made of P3HT-*b*-PNDIT2 BCPs after melt-recrystallization of the P3HT block at 250°C.[3]

The strong crystallization incompatibility between the two blocks in P3HT-*b*-PNDIT2 is very different from e.g. PE-*b*-sPP.[24] Here, a chain tilt of 37° between PE and sPP helps to adjust the area par junction at the PE/sPP interface and thus to overcome the lattice mismatch between the two blocks. This situation is not observed for P3HT-*b*-PNDIT2 because of the strong rigidity of the conjugated polymer backbone as compared to the flexible polyolefin chains in PE-*b*-sPP. This high backbone rigidity is also at the origin of the simultaneous alignment of P3HT and PNDIT2 blocks by HT rubbing. At that point it is worth to note that the presence of a single DPP unit at the block junction is apparently not able to favor self-organization of the copolymers and cannot balance the mismatch in lattice parameters between P3HT and PNDIT2. In place of DPP, the introduction of a short, non-conjugated flexible spacer between P3HT and PNDIT2 blocks might allow to counterbalance the lattice mismatch at the block junction, as it would allow for a relative chain tilt between the two blocks. We further envision that the substitution of the P3HT block with poly(3-decylthiophene) or poly(3-dodecylthiophene) having a larger layer spacing close to that of PNDIT2 could lead to more ordered interfaces and promote long-range ordering. As demonstrated by TEM and temperature-dependent UV-vis absorption spectroscopy, the difference in melting temperature between the two blocks is a second essential parameter that influences the morphology in all-conjugated copolymer as it will determine the contact plane of the blocks and the dominant polymorph. Clearly, a crystallization regime must be found such that both blocks can be either face-on or edge-on oriented on the substrate. For

$T_R \geq 200°C$, rubbed films are composed of face-on PNDIT2 in form II and edge-on oriented P3HT. This edge-on/face-on orientation of the two blocks may further lead to a strong frustration in the relative chain packing for both blocks, leading to extended disordered interfacial zones between P3HT and PNDIT2 segments. Purely edge-on oriented copolymers are not even observed for films annealed at 250°C. Temperatures beyond 300°C might be necessary to fully reorient the PNDIT2 block to edge-on. However, such high annealing temperature would lead to a loss of in-plane orientation of the copolymer.

## IV. Conclusion

All-conjugated donor-acceptor copolymers P3HT-*b*-PNDIT2 were successfully oriented in thin films using either epitaxy on TCB or high-temperature rubbing. It is possible to control the crystallization of the two blocks, i.e. their in-plane orientation, their polymorphism and their contact plane by choosing the orientation method as well as the crystallization temperature. Rubbing at $T_R = 175°C$ leads to long-range oriented lamellar morphologies with very high in-plane orientations and dominant face-on orientation of both P3HT and PNDIT2 blocks. Such morphology is considered ideal for charge injection into the electrodes of photovoltaic devices and cannot be obtained using conventional processing and annealing protocols.[3] In strong contrast, epitaxy on TCB leads to a preferential crystallization and orientation of the only P3HT block. Thermal annealing of epitaxied films is necessary to trigger the crystallization of the PNDIT2 block in form II. Crystallization of the PNDIT2 block constraints the lattice of the P3HT block and causes a substantial lattice expansion along the alkyl side chains. This lattice mismatch between the two blocks hampers the growth of long-range highly ordered lamellar domains and results in highly disordered interfaces at the block junction. Overall, this study underlines the necessity to adapt layer spacings along alkyl side chains between donor and acceptor blocks to minimize unit cell mismatches and

thus enhance long range self-assembly into ordered lamellar D-A phases. Besides electronic structure consideration, the molecular design of such all-conjugated block copolymers must therefore take into account the structural constraints at the block junction to enhance resulting growth and self-assembling properties that will equally control the photovoltaic properties in solar cell devices.

**Acknowledgments.**

We thank B. Lotz for fruitful discussions and reading of the manuscript. C. Blanck and M. Schmutz are gratefully acknowledged for technical support in TEM. P. Allgayer and L. Herrmann are acknowledged for the design and technical support with the rubbing machine. We thank gratefully the IRTG Soft Matter (FN, VU) and the Baden-Württemberg-Stiftung for financial support.

**Conflicts of interests.**

The authors declare no conflict of interest.

**Supporting information.**

Electron diffraction and bright field of P3HT block in oriented films, DSC curves of block copolymer and P3HT homopolymer, dependence of dichroic ratio with rubbing temperature, Lamellar morphology in oriented films observed in Bright Field TEM, Polarized UV-vis absorption spectra before/prior thermal annealing.

**References.**

(1) Sirringhaus, H.; Brown, P. J.; Friend, R. H.; Nielsen, M. M.; Bechgaard, K.; Langeveld-Voss, B. M. W.; Spiering, A. J. H.; Janssen, R. A. J.; Meijer, E. W.; Herwig, P. and de

Leeuw, D. M. Two-Dimensional Charge Transport in Self-Organized, High-Mobility Conjugated Polymers. *Nature* **1999**, *401*, 685.

(2) P3HT revisited – From molecular Scale to Solar Cell, S. Ludwigs Ed., 2014, Springer, p. 1-232.

(3) Nübling, F.; Hopper, T. R.; Kuei, B.; Komber, H.; Untilova, V.; Schmidt, S. B.; Brinkmann, M.; Gomez, E. D.; Bakulin, A. A.; Sommer, M. Block Junction-Functionalized All-Conjugated Donor–Acceptor Block Copolymers. *ACS Appl. Mater. Interfaces* **2019**, *11* (1), 1143–1155.

(4) Fabiano, S.; Yoshida, H.; Chen, Z.; Facchetti, A.; Loi, M. A. Orientation-Dependent Electronic Structures and Charge Transport Mechanisms in Ultrathin Polymeric n-Channel Field-Effect Transistors. *ACS Appl. Mater. Interfaces* **2013**, *5* (10), 4417–4422.

(5) Kang, H.; Kim, K.-H.; Choi, J.; Lee, C.; Kim, B. J. High-Performance All-Polymer Solar Cells Based on Face-On Stacked Polymer Blends with Low Interfacial Tension. *ACS Macro Lett.* **2014**, *3* (10), 1009–1014.

(6) Schuettfort, T.; Huettner, S.; Lilliu, S.; Macdonald, J. E.; Thomsen, L.; McNeill, C. R. Surface and Bulk Structural Characterization of a High-Mobility Electron-Transporting Polymer. *Macromolecules* **2011**, *44*, 1530–1539.

(7) Jung, J.; Lee, W.; Lee, C.; Ahn, H.; Kim, B. J. Controlling Molecular Orientation of Naphthalenediimide-Based Polymer Acceptors for High Performance All-Polymer Solar Cells. *Advanced Energy Materials* **2016**, *6* , 1600504.

(8) a) Yuan, J.; Zhang, Y.; Zhou, L.; Zhang, G.; Yip, H.-L.; Lau, T.-K.; Lu, X.; Zhu, C.; Peng, H.; Johnson, P. A.; et al. Single-Junction Organic Solar Cell with over 15% Efficiency Using Fused-Ring Acceptor with Electron-Deficient Core. *Joule* **2019**. https://doi.org/10.1016/j.joule.2019.01.004. b) Fan, B.; Zhang, D.; Li, M.; Zhong, W.; Zeng, Z.; Ying, L.; Huang, F.; Cao, Y. Achieving over 16% Efficiency for Single-Junction Organic Solar Cells. *Science China Chemistry* **2019**. https://doi.org/10.1007/s11426-019-9457-5. c)Meng, L.; Zhang, Y.; Wan, X.; Li, C.; Zhang, X.; Wang, Y.; Ke, X.; Xiao, Z.; Ding, L.; Xia, R.; et al. Organic and Solution-Processed Tandem Solar Cells with 17.3% Efficiency. *Science* **2018**, *361* (6407), 1094.

(9) Huang, Y.; Kramer, E. J.; Heeger, A. J.; Bazan, G. C. Bulk Heterojunction Solar Cells: Morphology and Performance Relationships. *Chem. Rev.* **2014**, *114*, 7006–7043.

(10) Ye, L.; Hu, H.; Ghasemi, M.; Wang, T.; Collins, B. A.; Kim, J.-H.; Jiang, K.; Carpenter, J. H.; Li, H.; Li, Z.; et al. Quantitative Relations between Interaction Parameter, Miscibility and Function in Organic Solar Cells. *Nature Materials* **2018**, *17*, 253–260.

(11) Chou, K. W.; Yan, B.; Li, R.; Li, E. Q.; Zhao, K.; Anjum, D. H.; Alvarez, S.; Gassaway, R.; Biocca, A.; Thoroddsen, S. T.; et al. Spin-Cast Bulk Heterojunction Solar Cells: A Dynamical Investigation. *Advanced Materials* **2013**, *25*, 1923–1929.

(12) Wang, G.; Melkonyan, F. S.; Facchetti, A.; Marks, T. J. All-Polymer Solar Cells: Recent Progress, Challenges, and Prospects. *Angewandte Chemie International Edition* **2018**, *58*, *4129*.

(13) Verduzco, R.; Botiz, I.; Pickel, D. L.; Kilbey, S. M.; Hong, K.; Dimasi, E.; Darling, S. B. Polythiophene-Block-Polyfluorene and Polythiophene-Block-Poly(Fluorene-Co-Benzothiadiazole): Insights into the Self-Assembly of All-Conjugated Block Copolymers. *Macromolecules* **2011**, *44*, 530–539.

(14) Zhang, Y.; Tajima, K.; Hashimoto, K. Nanostructure Formation in Poly(3-Hexylthiophene-Block-3-(2-Ethylhexyl)Thiophene)S. *Macromolecules* **2009**, *42*, 7008–7015.

(15) Lohwasser, R. H.; Gupta, G.; Kohn, P.; Sommer, M.; Lang, A. S.; Thurn-Albrecht, T.; Thelakkat, M. Phase Separation in the Melt and Confined Crystallization as the Key to Well-Ordered Microphase Separated Donor–Acceptor Block Copolymers. *Macromolecules* **2013**, *46*, 4403–4410.

(16) Scherf, U.; Gutacker, A.; Koenen, N. All-Conjugated Block Copolymers. *Acc. Chem. Res.* **2008**, *41*, 1086–1097.

(17) Segalman, R. A.; McCullouch, B.; Kirmayer, S. and Urban , J. J. Block Copolymers for Organic Optoelectronics. *Macromolecules* **2009**, *42*, 9205–9216.

(18) Lee, Y.; Gomez, E. D. Challenges and Opportunities in the Development of Conjugated Block Copolymers for Photovoltaics. *Macromolecules* **2015**, *48*, 7385–7395.

(19) Shaw, P. E.; Ruseckas, A.; Samuel, I. D. W. Exciton Diffusion Measurements in Poly(3-Hexylthiophene). *Advanced Materials* **2008**, *20*, 3516–3520.

(20) Sary, N.; Richard, F.; Brochon, C.; Leclerc, N.; Lévêque, P.; Audinot, J.-N.; Berson, S.; Heiser, T.; Hadziioannou, G.; Mezzenga, R. A New Supramolecular Route for Using Rod-Coil Block Copolymers in Photovoltaic Applications. *Advanced Materials* **2010**, *22*, 763–768.

(21) Barrau, S.; Heiser, T.; Richard, F.; Brochon, C.; Ngov, C.; van de Wetering, K.; Hadziioannou, G.; Anokhin, D. V.; Ivanov, D. A. Self-Assembling of Novel Fullerene-Grafted Donor–Acceptor Rod−Coil Block Copolymers. *Macromolecules* **2008**, *41*, 2701–2710.

(22) Zhang, Q.; Cirpan, A.; Russell, T. P.; Emrick, T. Donor−Acceptor Poly(Thiophene-Block-Perylene Diimide) Copolymers: Synthesis and Solar Cell Fabrication. *Macromolecules* **2009**, *42*, 1079–1082.

(23) Sommer, M.; Lang, A. S.; Thelakkat, M. Crystalline–Crystalline Donor–Acceptor Block Copolymers. *Angewandte Chemie International Edition* **2008**, *47*, 7901–7904.

(24) De Rosa, C.; Di Girolamo, R.; Auriemma, F.; D'Avino, M.; Talarico, G.; Cioce, C.; Scoti, M.; Coates, G. W.; Lotz, B. Oriented Microstructures of Crystalline–Crystalline Block Copolymers Induced by Epitaxy and Competitive and Confined Crystallization. *Macromolecules* **2016**, *49*, 5576–5586.

(25) Smith, K. A.; Stewart, B.; Yager, K. G.; Strzalka, J.; Verduzco, R. Control of All-Conjugated Block Copolymer Crystallization via Thermal and Solvent Annealing. *Journal of Polymer Science Part B: Polymer Physics* **2014**, *52*, 900–906.

(26) Smith, K. A.; Lin, Y.-H.; Dement, D. B.; Strzalka, J.; Darling, S. B.; Pickel, D. L.; Verduzco, R. Synthesis and Crystallinity of Conjugated Block Copolymers Prepared by Click Chemistry. *Macromolecules* **2013**, *46*, 2636–2645.

(27) Wang, J.; Ueda, M.; Higashihara, T. Synthesis and Morphology of All-Conjugated Donor–Acceptor Block Copolymers Based on Poly(3-Hexylthiophene) and Poly(Naphthalene Diimide). *Journal of Polymer Science Part A: Polymer Chemistry* **2014**, *52*, 1139–1148.

(28) Wang, J.; Ueda, M.; Higashihara, T. Synthesis of All-Conjugated Donor–Acceptor–Donor ABA-Type Triblock Copolymers via Kumada Catalyst-Transfer Polycondensation. *ACS Macro Lett.* **2013**, *2*, 506–510.

(29) Nakabayashi, K.; Mori, H. All-Polymer Solar Cells Based on Fully Conjugated Block Copolymers Composed of Poly(3-Hexylthiophene) and Poly(Naphthalene Bisimide) Segments. *Macromolecules* **2012**, *45*, 9618–9625.

(30) Yang, H.; Zhang, R.; Wang, L.; Zhang, J.; Yu, X.; Liu, J.; Xing, R.; Geng, Y.; Han, Y. Face-On and Edge-On Orientation Transition and Self-Epitaxial Crystallization of All-Conjugated Diblock Copolymer. *Macromolecules* **2015**, *48*, 7557–7566.

(31) Schubert, M.; Collins, B. A.; Mangold, H.; Howard, I. A.; Schindler, W.; Vandewal, K.; Roland, S.; Behrends, J.; Kraffert, F.; Steyrleuthner, R.; Chen, Z.; Fostiropoulos, K.; Bittl, R.; Salleo, A.; Facchetti, A.; Laquai, F.; Ade, H. W. and Neher, D. Correlated Donor/Acceptor Crystal Orientation Controls Photocurrent Generation in All-Polymer Solar Cells. *Advanced Functional Materials* **2014**, *24*, 4068–4081.

(32) Hamidi-Sakr, A.; Biniek, L.; Fall, S.; Brinkmann, M. Precise Control of Lamellar Thickness in Highly Oriented Regioregular Poly(3-Hexylthiophene) Thin Films Prepared by High-Temperature Rubbing: Correlations with Optical Properties and Charge Transport. *Advanced Functional Materials* **2016**, *26*, 408–420.

(33) Brinkmann, M.; Wittmann, J. C. Orientation of Regioregular Poly(3-Hexylthiophene) by Directional Solidification: A Simple Method to Reveal the Semicrystalline Structure of a Conjugated Polymer. *Advanced Materials* **2006**, *18*, 860.

(34) Brinkmann, M.; Gonthier, E.; Bogen, S.; Tremel, K.; Ludwigs, S.; Hufnagel, M.; Sommer, M. Segregated versus Mixed Interchain Stacking in Highly Oriented Films of Naphthalene Diimide Bithiophene Copolymers. *ACS Nano* **2012**, *6*, 10319–10326.

(35) Tremel, K.; Fischer, F. S. U.; Kayunkid, N.; Di Pietro, R.; Tkachov, R.; Kiriy, A.; Neher, D.; Ludwigs, S.; Brinkmann, M. Charge Transport Anisotropy in Highly Oriented Thin Films of the Acceptor Polymer P(NDI2OD-T2). *Advanced Energy Materials* **2014**, *4*, 1301659.

(36) Brinkmann, M.; Rannou, P. Molecular Weight Dependence of Chain Packing and Semicrystalline Structure in Oriented Films of Regioregular Poly(3-Hexylthiophene) Revealed by High-Resolution Transmission Electron Microscopy. *Macromolecules* **2009**, *42*, 1125–1130.

(37) Biniek, L.; Pouget, S.; Djurado, D.; Gonthier, E.; Tremel, K.; Kayunkid, N.; Zaborova, E.; Crespo-Monteiro, N.; Boyron, O.; Leclerc, N.; Ludwigs, S. and Brinkmann, M. High-Temperature Rubbing: A Versatile Method to Align Pi-Conjugated Polymers without Alignment Substrate. *Macromolecules* **2014**, *47*, 3871–3879.

(38) Matsidik, R.; Komber, H.; Sommer, M. Rational Use of Aromatic Solvents for Direct Arylation Polycondensation: C–H Reactivity versus Solvent Quality. *ACS Macro Lett.* **2015**, *4*, 1346–1350.

(39) Nübling, F.; Komber, H.; Sommer, M. All-Conjugated, All-Crystalline Donor–Acceptor Block Copolymers P3HT-*b*-PNDIT2 via Direct Arylation Polycondensation. *Macromolecules* **2017**, *50*, 1909–1918.

(40) Sommer, M. Conjugated Polymers based on Naphthalene Diimide for Organic Electronics *J. Mater. Chem. C*, **2014**, 2, 3088-3098.

(41) Manson, J. A. and L. H. Sperling in Polymer Blends and Composites, Plenum Press, New York, 1976, p. 169.

(42) Lotz, B.; Kovacs, A. J.; Bassett, G. A.; Keller, A. *Kolloid Z. Z. Polym.* **1966**, *209*, 115.

(43) Yang, C.; Orfino, F. P.; Holdcroft, S. A Phenomenological Model for Predicting Thermochromism of Regioregular and Nonregioregular Poly(3-Alkylthiophenes). *Macromolecules* **1996**, *29*, 6510–6517.

(44) Seeboth, A.; Lötzsch, D.; Ruhmann, R.; Muehling, O. Thermochromic Polymers—Function by Design. *Chem. Rev.* **2014**, *114*, 3037–3068.

Graphic for manuscript